ACS Energy LETTERS

Cite This: ACS Energy Lett. 2018, 3, 65−71

LETTER

Asymmetric K/Li-Ion Battery Based on Intercalation Selectivity

Jiaxin Zheng,[†,⊥] Wenjun Deng,[†,⊥] Zongxiang Hu,[†,⊥] Zengqing Zhuo,[†,‡] Fusheng Liu,[‡] Haibiao Chen,[†] Yuan Lin,[†] Wanli Yang,[§] Khalil Amine,[∥] Rui Li,[*,†] Jun Lu,[*,∥] and Feng Pan[*,†]

[†]School of Advanced Materials, Shenzhen Graduate School, Peking University, Shenzhen 518055, People's Republic of China

[‡]Advanced Light Source, Lawrence Berkeley National Laboratory, Berkeley, California 94720, United States

[§]College of Materials Science and Engineering, Shenzhen University and Shenzhen Key Laboratory of Special Functional Materials, Shenzhen 518060, People's Republic of China

[∥]Electrochemical Technology Program, Chemical Sciences and Engineering Division, Argonne National Laboratory, Argonne, Illinois 60439, United States

Supporting Information

ABSTRACT: Using ab initio calculations combined with experimental confirmation, we design an asymmetric intercalation battery using $K_2NiFe^{II}(CN)_6$ as the cathode, commercial graphite as the anode, and an organic electrolyte containing mixed lithium and potassium salts. It works by reversible K-ion intercalation at the cathode side and reversible Li-ion intercalation at the anode side simultaneously. The π-electron coordination environment in $K_2NiFe^{II}(CN)_6$ ensures the preferred reversible intercalation of the K-ion, and the small ionic radius ensures the preferred reversible intercalation of the Li-ion in graphite. It also shows a high working voltage (~3.6 V) and an ultralong cycling life with no capacity fading even after 5000 cycles.

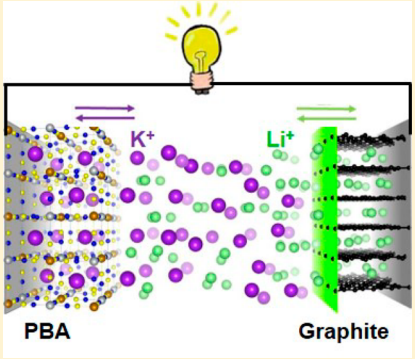

Due to the natural abundance and low cost compared with lithium, the potassium-ion battery (PIB) shows great potential to be used in grid storage,[1−5] where a fast charge/discharge rate (CDR) and long cycling life are required. Recently, Prussian Blue and its analogues (PBAs) with the capability of reversible intercalation of K^+ were demonstrated to be an attractive cathode candidate for PIBs,[2,4−10] featuring excellent cycling performance. Other materials including $FeSO_4F$,[11] $KTiPO_4O$,[12] and $AVPO_4F$[13] were also demonstrated encouraging capacity and cycling life on the cathode side. Further development of such materials toward practical PIBs, however, remains a big challenge, largely due to the limited choices of K^+-intercalation anodes.[1,3,14] Though graphite has been recently reported to be able to store K^+ and deliver a high capacity of around 273 mAh/g through a similar intercalation mechanism as that of Li^+, its capacity retention and rate capability fall far short of practical application.[15] The relatively large volume change during the discharge and charge (about 60% expansion for K-ion intercalation in graphite,[16] while only 12% expansion for Li-ion storage in graphitic[17]) is mainly responsible for such performance degradation. Metallic potassium, on the other hand, could be an ideal choice of anode for PIBs in terms of energy density. However, due to the much higher reactivity than lithium metal, it is more difficult to address the challenge facing potassium metal. Recent advances reported that graphitizable soft carbon[18] and nongraphitizable hard carbon spheres (HCSs)[19] as anodes for PIBs show high specific capacities (273 mAh^{-1} for the soft carbon and 262 $mAhg^{-1}$ for HCSs) and improved cycling stability compared with graphite. Especially, HCSs exhibited, to date, the best cycling stability among graphite, soft carbon, and hard carbon, where the electrode retained 83% of its initial capacity after 100 cycles at C/10.[19] Exploring stable and reversible anodes beyond a conventional category is of great interest to adjust the electrochemistry fitting well with a potassium cathode. However, the mission is very challenging due to the lack of a qualified candidate with high potassium storage capability and extraordinary stability, as well as the sluggish kinetics of K^+ intercalating into the electrode host material.

Different from the traditional way, here we design an asymmetric cell to work by reversible intercalation of K^+ at the cathode side and a different ion (e. g., Li^+) at the anode side. This would not only extend the choice of anode materials but also be interesting from a fundamental perspective. To realize

Received: October 18, 2017
Accepted: November 27, 2017
Published: November 27, 2017

Downloaded via UNIV TOWN OF SHENZHEN on March 13, 2026 at 06:14:06 (UTC).
See https://pubs.acs.org/sharingguidelines for options on how to legitimately share published articles.

© 2017 American Chemical Society

DOI: 10.1021/acsenergylett.7b01021
ACS Energy Lett. 2018, 3, 65−71

this concept, we need to choose appropriate electrode materials showing thermodynamic or kinetic priority for intercalation of a targeted cation as well as excellent cycling stability. The thermodynamic priority mainly depends on the reaction energy and chemical potential for cation storage in the electrode materials at a certain temperature and pressure, which is correlated with the kind of redox couples for transition metals and the cation coordination environments.[20] The kinetic priority mainly depends on the cation diffusion ability inside of the bulk phase, as well as the nature and level of phase transition behavior of an electrode with a certain specific surface area. Strongly dependent on the smaller ionic radius of the Li-ion, various traditional intercalation electrode materials usually show a kinetic priority for Li^+ intercalation. By introducing Li-ions into the PIB, the system would benefit synergistically by taking the electrochemical advantages of both Li^+ and K^+. The ultimate request for choosing the candidates of the cathode for K^+ and anode for Li^+ should be both kinetically and thermodynamically favorable.

By using ab initio calculations combined with experiments, we demonstrate that the π-electron coordination environment in PBAs can improve the potential for alkali cation storage with larger size ($V_{Li} < V_{Na} < V_K$ vs Li/Li^+). Such a trend is different from the p orbital hybridization coordination environment of oxygen in layered transition metal oxides and polyanion structures. It indeed shows thermodynamic priority of K-ion reversible intercalation. Considering the kinetic priority for Li intercalation with little volume expansion in graphite, we constructed a facile asymmetric intercalation battery using a $K_2NiFe^{II}(CN)_6$ (a kind of PBA) cathode, commercial graphite anode, and organic electrolyte with mixed KPF_6 and $LiPF_6$. This battery showed simultaneously reversible K^+ and Li^+ intercalation at the cathode and anode sides, respectively.

PBAs possess a well-known perovskite-like face-centered cubic crystal structure in the $Fm\bar{3}m$ space group and the general chemical formula of $A_xM_aM_b(CN)_6{\cdot}nH_2O$ (A = alkali cations and M = Ni, Co, Mn, Fe, Cu, Zn).[4,21−23] Among them, hexacyanoferrates (M_b = Fe) with iron atoms coordinated at the carbon end under low spin states and M_a atoms coordinated at the nitrogen end are low-cost and easy-access. Therefore, such crystals are most widely studied and considered superior over other PBAs as electrode candidates. Different from the oxygen coordination environment for alkali cation storage in the traditional cathode materials (e. g., olive $FePO_4$ and layered transition metal oxide), alkali cations always coordinate with 12 CN ligands via π-electrons in PBAs. To elucidate the difference of the alkali cation storage between oxygen coordination and π-electron coordination in PBAs, ab initio calculations were employed to study their electrochemical properties. Figure 1 shows the structure models of cubic α-$AFePO_4$, $ACoO_2$, and $A_4Ni_4[Fe(CN)_6]_4$ (NiHCF, a kind of PBA) (A = Li, Na, K). Similar as previous works,[24−26] the coordinating waters were not considered in the structure models of $A_4Ni_4[Fe(CN)_6]_4$ due to the uncertainty of position determination (Figure 1c). Without coordinating waters, such a model is still helpful to provide qualitative insight into the difference of alkali cation storage between oxygen coordination and π-electron coordination.

Previous theoretical works have studied the electronic structures of FeHCF, MnHCF, and CoHCF and revealed the mechanism for spin-crossover phenomenon in these materials caused by temperature-induced or photoinduced charge-transfer excitation.[24,27−29] However, a theoretical study on

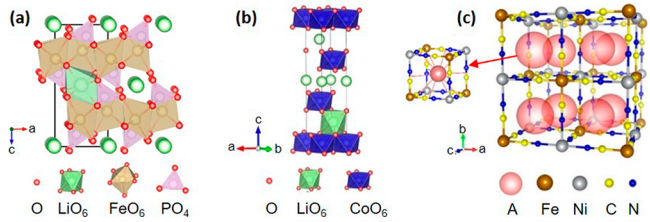

Figure 1. 3D crystal structures of $LiFePO_4$ (a), $LiCoO_2$ (b), and $A_4Ni_4[Fe(CN)_6]_4$ (c). $LiCoO_2$ and $LiFePO_4$ possess an octahedron oxygen coordination environment for Li-ion storage. The Wyckoff sites 8c in $A_4Ni_4[Fe(CN)_6]_4$ are occupied by A-ions (Li^+, Na^+, and K^+). Alkali cations coordinate with 12 CN ligands by π-electrons in $A_4Ni_4[Fe(CN)_6]_4$.

the fully periodic NiHCF is still lacking, except experimental reports on the basic electrochemical charge/discharge behavior of this cathode for KIBs.[4,30] Here we first calculated the electronic structure of lithiated NiHCF (Figure 2a). The

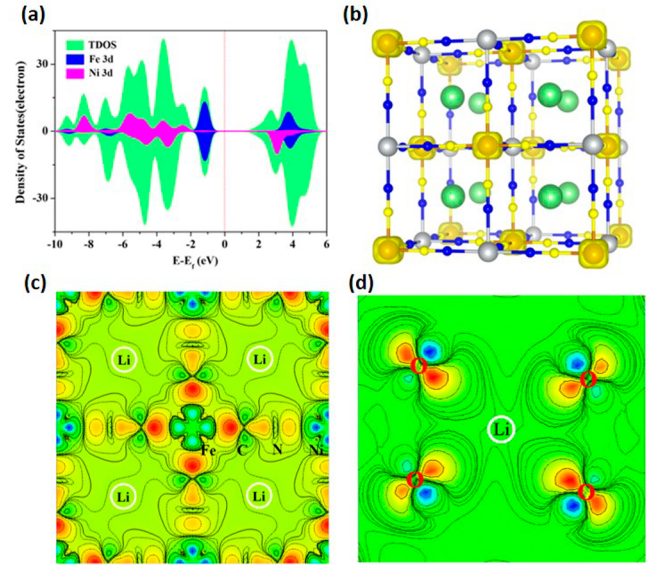

Figure 2. (a) Total density of states (DOS) and projected DOS of NiHCF ($Li_2NiFe^{II}(CN)_6$). (b) Calculated Bloch wave function approaching the Fermi level for NiHCF. Green ball, Li; brown, Fe; silver, Ni; blue, N; yellow, C. (c) Charge density difference section along the (001) plane of NiHCF. (d) Charge density difference section along the (010) plane of $LiFePO_4$. The blue and red represent electron depletion and accumulation, respectively.

occupied low-spin Fe 3d orbitals are clearly observed from the highest occupied states. The Bloch wave function approaching the Fermi level shows that the wave function locates at iron and the morphologies of these functions are all similar to typical atomic d orbitals (Figure 2b).[31] Obviously, during the charging state, the Fermi energy level will gradually drop down toward valence bands composed of Fe t_{2g} due to electron transfer. By contrast, the 3d states of nickel ions are located far below the Fermi level (Figure 2a), indicating hard charge transfer (oxidation) of nickel ions during delithiation. All of these results were confirmed by our later X-ray photoelectron spectroscopy (XPS) and soft X-ray adsorption spectroscopy (sXAS) measurements. Furthermore, the plot of the charge density difference section along the (001) direction clearly manifests that the interstitial cations have an interaction with π-

DOI: 10.1021/acsenergylett.7b01021
ACS Energy Lett. 2018, 3, 65−71

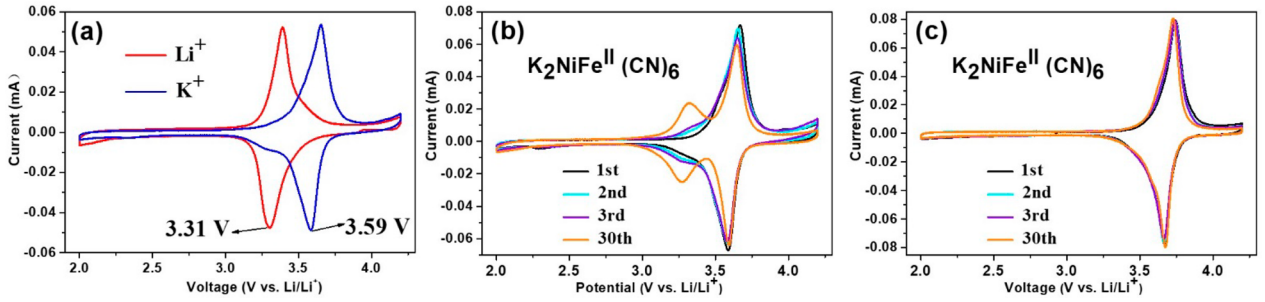

Figure 3. (a) CV profiles for Li- and K-ion storage in $K_2NiFe^{II}(CN)_6$. (b,c) CV profiles within a potential window of 2.0−4.2 V for $K_2NiFe^{II}(CN)_6$ as the initial cathode material in different electrolytes: (b) electrolyte containing only lithium salt, 1 M $LiPF_6$ in EC/DMC (1:1, v/v); (c) electrolyte containing mixed lithium and potassium salt, 0.5 M KPF_6 and 0.5 M $LiPF_6$ in EC/DMC (1:1, v/v). The scan rates in the three cases are 0.1 mv s^{-1}. All of the potentials (vs corresponding reference electrodes) are converted to potentials (vs Li/Li^+) for convenient comparison.

electrons of CN ligands (Figure 2c). In other words, the frame structure bonds Li-ions via delocalized π-electrons of CN ligands at the corner of the structure. For comparison, Figure 2d shows a plot of the charge density difference section along the (010) direction of $LiFePO_4$, which clearly shows that the Li-ions bond with oxygen via heavy hybridization between the localized Li-s and O-p orbitals.

The average potentials for Li^+, Na^+, and K^+ storage in NiHCF, α-$AFePO_4$, and $ACoO_2$ were further calculated and follow an order of $V_{Li} < V_{Na} < V_K$ (vs Li/Li^+) in NiHCF (Table S1). It indicates that a larger cation size would lead to a higher storage potential under the same redox couple of Fe^{II}/Fe^{III} in PBAs. By contrast, for $AFePO_4$, the average potential for sodium storage (3.27 V vs Li/Li^+) is lower than that for lithium storage (3.55 V vs Li/Li^+). The trend for $ACoO_2$ is the same as that for $AFePO_4$. Because of the delocalization of π-orbitals, a larger cation size can lead to larger orbital overlap to improve the binding energy in PBAs. However, in oxygen coordination environments, due to the relative localization of p orbitals and short-range interaction, the bigger alkali cation size would lead to smaller hybridization between the p orbital of oxygen and the s orbital of alkali cation and lower potential for storage. Thus, the π-electron coordination environment would improve the potential for alkali cation storage with increased cation size.

To confirm the above calculations, we synthesized NiHCF ($K_2NiFe^{II}(CN)_6$) nanocrystals (section 2 in the SI) and performed cyclic voltammetry (CV) tests for Li^+- and K^+-ion storage. All of the tests were carried out at a scan rate of 0.1 mv s^{-1} within 2.0−4.2 V, and a lithium or potassium plate was used as the counter and reference electrodes. The initial $K_2NiFe^{II}(CN)_6$ electrode was initially charged to 4.2 V to remove K^+ and then was carefully washed three times before being assembled into the button cell for further CV tests. At this time, we can see the NiHCF electrode with K^+ extracted, showing only one sharp redox peak for all alkali cation storage tests (Figure 3a). Considering the small polarization between the oxidation peaks and reduction peaks, reduction peaks were used for comparison. As shown in Figure 3a, the reduction peaks at 3.31 and 3.59 V (vs Li/Li^+) were observed for intercalation Li- and K-ions, respectively. This confirms the trend given by theoretical calculations that the larger the alkali ionic radius, the higher the redox potential for storage in NiHCF. The reduction peak at 3.31 V (vs Li/Li^+) for intercalation of Li-ions is also consistent with previous experimental results.[32] The deviation between the experimentally measured and calculated potentials can be due to the excluded coordinating waters in the model: the lone pair electrons of water steadily coordinated to the frame can bond with alkali cations to improve the potential. We also synthesized another kind of NiHCF nanocrystals that contain almost no K-ion in the initial sample. The corresponding CV tests also confirm the trend derived by theoretical calculations (section 3 in the SI).

We can see that the K-ion storage shows a high thermodynamic priority of reversible intercalation in PBAs. The kinetics of reversible intercalation would not be a disadvantage for the K-ion due to the large interspace of PBAs. To prove these inferences, the CV curves of $K_2NiFe^{II}(CN)_6$ as the initial cathode material were measured in 1 M $LiPF_6$ in a mixture of ethylene carbonate (EC) and dimethyl carbonate (DMC) (1:1) (Figure 3b). The CV exhibits only a sharp redox peak at around 3.59 V (vs Li/Li^+) in the first few cycles, corresponding to the K^+ reversible intercalation. The small redox peak at around 3.31 V (vs Li/Li^+) after 30 cycles (Figure 3b) corresponds to a small content of Li^+ reversible intercalation. This inevitable intercalation of Li-ions into the PBA cathode after a certain number of cycles can be attributed to the electrolyte that we used: 1 M $LiPF_6$ in EC/DMC (1:1, v/v). The concentration of K^+ in the electrolyte is too low to avoid intercalation of a small content of Li-ions into the PBA cathode after several cycles. If the concentration of K^+ in the initial electrolyte is increased, the intercalation of a small content of Li-ions into the PBA cathode can be suppressed or avoided. To verify this, we changed the original electrolyte with a new EC/DMC (1:1, v/v) electrolyte containing 0.5 M KPF_6 and 0.5 M $LiPF_6$ mixed salt. The CV profiles within a potential window of 2.0−4.2 V for $K_2NiFe^{II}(CN)_6$ as the initial cathode material were recollected in this new electrolyte (Figure 3c). Compared with Figure 3b, we can see that the small redox peak at around 3.31 V (vs Li/Li^+) after 30 cycles corresponding to a small content of Li^+ reversible intercalation disappears in Figure 3c.

According to previous experimental and theoretical works,[16,33] though the K-ion storage shows a little thermodynamic priority (by about 0.1 V) in graphite, the kinetic priority for Li intercalation in graphite is more significant due to the small radius of the Li-ion. Here, we are able to design an asymmetric K/Li-ion full battery that consists of $K_2NiFe^{II}(CN)_6$ as the cathode, commercial graphite as the anode, and an EC/DMC (1:1, v/v) electrolyte containing mixed 0.5 M KPF_6 and 0.5 M $LiPF_6$ salt. The cathode/anode mass ratio was set to 4/1 (see details in the Methods section in

DOI: 10.1021/acsenergylett.7b01021
ACS Energy Lett. 2018, 3, 65−71

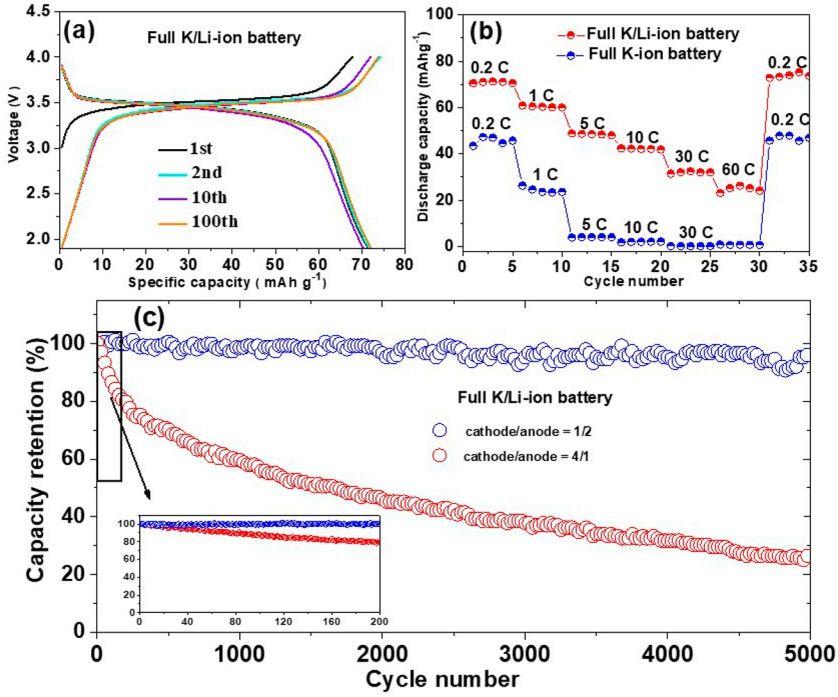

Figure 4. (a) Charge and discharge curves at different cycles at 0.2 C (1 C = 60 mA g^{-1}) for the full asymmetric K/Li-ion battery. (b) Discharge cycles for the full K/Li-ion battery and full K-ion battery at different current densities. The cathode/anode mass ratio is 4/1 in (a) and (b). (c) Capacity (per mass of cathode) retention versus cycle number at a current rate of 30 C for the full K/Li-ion batteries.

the SI), and the anode was prelithiated to avoid capacity loss during the formation of a solid electrolyte interphase (SEI). Figure 4a shows the charge−discharge curves of this battery at a low current rate of 0.2 C (1 C = 60 mA g^{-1}) at different cycles from 2.0 to 4.0 V. There is a main average charge−discharge voltage platform at around 3.6 V (vs Li/Li^+), corresponding to K^+ deintercalation. The charge−discharge curves are consistent with the CV results in Figure 3b (the sharp redox peak at around 3.59 V). Though Li insertion is hardly found from the electrochemical charge−discharge curves, there is still small content of Li-ion insertion in the PBA cathode, which is revealed by further XPS measurements on the PBA cathode discharged to 2.0 V after 50 cycles (Figure S10). After 100 cycles, the discharge capacity (per mass of cathode) is 71.2 mAh g^{-1}, close to the theoretical specific capacity (70.7 mAh g^{-1})[30] for $K_2NiFe^{II}(CN)_6$. Our XPS and sXAS measurements show that during charging, Fe^{II} is oxidized to Fe^{III} while the valence state of Ni remain unchanged (section 4 in the SI), consistent with the calculations. We also fabricated a full K-ion battery for comparison, using the same $K_2NiFe^{II}(CN)_6$ cathode, the graphite anode, and KPF_6 in a mixture of EC and DMC (1:1) as the electrolyte. Compared with the full K/Li-ion battery, the full K-ion battery showed poor rate performance (Figure 4b). This indicates the kinetic limit at the anode and confirms the priority of Li-ion reversible intercalation at the anode in the full K/Li battery. In addition, our XPS measurements also confirmed the priority of Li-ion reversible intercalation at the graphite anode (Figure S10).

Increasing the anode mass of this full K/Li battery can further improve the rate performance. From Figure S11a, we can see that when the cathode/anode mass ratio was set to 1/2, the rate performance of the full K/Li-ion battery was improved by a large degree. The discharge capacity (per mass of cathode) of 51.7 mAh g^{-1} (72.6% of the capacity at 0.2 C) was obtained even at 30 C. Moreover, this new full K/Li-ion battery showed greatly improved cycling stability. For the original full K/Li-ion battery with a cathode/anode mass ratio of 4/1, the capacity retention decreased to 80% after 200 cycles, but the new full K/Li-ion battery with a cathode/anode mass ratio of 1/2 showed no obvious capacity decay even after 5000 cycles (Figure 4c). The greatly improved rate capability and cycling stability can be attributed to when the cathode/anode mass ratio was set to 1/2, the total capacity of Li-ion storage in the anode exceeded the total capacity of K-ion storage in the cathode by around 8 times. During electrochemical cycling, only the shallow intercalation/deintercalation of Li-ions in graphite is needed; therefore, the rate capability and the cycling performance are mainly determined by the cathode side. Due to the large interspace and robust MOF structure for K-ion intercalation in PBAs, the whole rate capability and cycling performance of this full K/Li-ion battery are greatly improved.

This asymmetric K/Li-ion battery employs the preferred intercalation of K^+ in the cathode and the preferred intercalation of Li^+ in the anode. The excellent cycling performance can be attributed to two reasons: (1) the robust MOF structure[4,7−10] and the smaller radius of $Fe(CN)_6^{4-}$ than that of $Fe(CN)_6^{3-}$ during its oxidation:[34] the Fe^{II} has very strong π-back-bonding to the carbon of the cyanide ion,[34] thus leading to a small volume change (2.1%) of the unit cell (Figure S12); (2) the high kinetic priority of Li^+ in graphite ensures stable intercalation at the anode with little volume expansion. The high priority also ensures the sluggish kinetics of this battery. Compared with the conventional PBA Li-ion batteries (LIBs), the specific capacities are similar, but the working voltage is improved by 0.28 V in this full K/Li-ion battery. Because only the low-spin iron accounts for the redox couples (Fe^{II}/Fe^{III}) during deintercalation, the capacity of this K/Li-ion asymmetric battery can also be improved by changing the nitrogen-coordinated transition metal with Cu, Mn, and Fe for

DOI: 10.1021/acsenergylett.7b01021
ACS Energy Lett. 2018, 3, 65−71

alkali cation storage by introducing extra Cu(I)/(II),[35−37] Mn(III)/(II),[23,38,39] and high-spin Fe(II)/(III) redox couples.[40]

Similar dual-ion batteries have also been explored in either aqueous or nonaqueous electrolytes before.[41−57] Such dual-ion batteries can be divided into two classes: one class works by reversible intercalation of anion A (e. g., PF_6^-) at the cathode side and reversible intercalation of cation B (e. g., Li^+) at the anode side;[45−49] the second class works by reversible intercalation/conversion of cation A (e. g., Na^+) at the cathode side and reversible intercalation/conversion of cation B (e. g., Mg^{2+}) at the anode side.[42−44,50−57] Compared to the traditional LIBs, the first class of dual-ion batteries shows good potential application as promising energy storage devices due to a higher working voltage (mainly above 4.5 V), low cost, good safety, and environmental friendliness, but they face the challenge of limited choices of cathode materials to host the anions. The second class of dual-ion systems shows greatly extended choices of cathode and anode materials and can combine their respective advantages. For example, a reported Al^{3+}/Li^+ dual-ion battery (using a $LiFePO_4$ cathode, aluminum anode, and acidic ionic liquid electrolyte) works by reversible Li-ion intercalation into $LiFePO_4$ and reversible aluminum deposition/stripping at the aluminum anode.[42] The safe nature and earth abundance of aluminum coupled with the safety of ionic liquid electrolytes make this new kind of hybrid battery very attractive for grid and stationary applications. The reported Mg^{2+}/Li^+ (refs 50−57) and Mg^{2+}/Na^+ (refs 41, 43, and 44) dual-ion batteries work by Li^+/Na^+ reversible conversion reaction (or intercalation) at the cathode compound side and irreversible deposition/stripping of Mg at the metallic magnesium anode side due to the preferred sodiation over magnesiation (or preferred Li^+/Na^+ intercalation) at the cathode and preferred reversible Mg deposition−dissolution at the anode.[43] This dual-ion design could combine the advantages of the Mg metal anode and the Li^+/Na^+ intercalation cathode to provide much better safety, rate capability, and cycling stability. One problem for the reported second class of dual-ion (dual-cation) batteries is the limited working voltage. For example, due to the high redox potential of Al^{3+}/Al, the discharge potential of the Al^{3+}/Li^+ dual-ion battery is limited to 1.3 V.[42] Because of the high redox potential of Mg^{2+}/Mg, the working potentials of Mg^{2+}/Li^+ (ref 55) and Mg^{2+}/Na^+ (refs 41, 43, and 44) dual-ion batteries are limited to ∼1.2 and 1.1−2.6 V, respectively.

Compared with the above-reported dual-ion (dual-cation) batteries, our proposed asymmetric K/Li-ion battery works by reversible K-ion intercalation at the cathode side and reversible Li-ion intercalation at the anode side simultaneously, which is different from the above Mg^{2+}/Li^+ and Mg^{2+}/Na^+ dual-ion battery working by reversible Mg deposition−dissolution at the anode and Al^{3+}/Li^+ dual-ion battery working by reversible aluminum deposition/stripping at the anode. Due to the low potential for Li-ion storage and stable Li-ion intercalation in the graphite anode, our asymmetric K/Li-ion battery shows a much higher working voltage (∼3.6 V) and much better cycling performance than all of the above dual-ion batteries. In addition, we also for the first time demonstrated that the π-electron coordination environment in PBAs can improve the potential for alkali cation storage with larger size ($V_{Li} < V_{Na} < V_K$ vs Li/Li^+), which ensures the thermodynamic priority of K-ion reversible intercalation in PBAs. Such a trend is different from the p orbital hybridization coordination environment of oxygen in layered transition metal oxides and polyanion structures.

In summary, on the basis of the preferred reversible intercalation of K-ion in $K_2NiFe^{II}(CN)_6$ and the preferred reversible intercalation of Li-ion in graphite, we designed an asymmetric intercalation battery. This battery works well with simultaneous reversible K-ion intercalation at the cathode side and reversible Li-ion intercalation at the anode side and shows promoted electrochemical performance. This work shares guidance to extend the scope of future battery designs.

■ ASSOCIATED CONTENT

Supporting Information

The Supporting Information is available free of charge on the ACS Publications website at DOI: 10.1021/acsenergylett.7b01021.

More details about ab initio calculations and experiments (PDF)

■ AUTHOR INFORMATION

Corresponding Authors

*E-mail: lirui@pkusz.edu.cn (R.L.).
*E-mail: junlu@anl.gov (J.L.).
*E-mail: panfeng@pkusz.edu.cn (F.P.).

ORCID

Wanli Yang: 0000-0003-0666-8063
Khalil Amine: 0000-0001-9206-3719
Rui Li: 0000-0001-5480-8089
Jun Lu: 0000-0003-0858-8577
Feng Pan: 0000-0002-8216-1339

Author Contributions

⊥J.Z., W.D., and Z.H. contributed equally to this work.

Notes

The authors declare no competing financial interest.

■ ACKNOWLEDGMENTS

The research was financially supported by the National Materials Genome Project (2016YFB0700600), the National Natural Science Foundation of China (No. 21603007), and Shenzhen Science and Technology Research Grant (No. JCYJ20150729-111733470, JCYJ20151015162256516). This work was also supported by the U.S. Department of Energy under Contract DE-AC0206CH11357 with support provided by the Vehicle Technologies Office, Department of Energy (DOE) Office of Energy Efficiency and Renewable Energy (EERE).

■ REFERENCES

(1) Eftekhari, A.; Jian, Z.; Ji, X. Potassium Secondary Batteries. *ACS Appl. Mater. Interfaces* **2017**, *9*, 4404−4419.
(2) Su, D.; McDonagh, A.; Qiao, S.-Z.; Wang, G. High-Capacity Aqueous Potassium-Ion Batteries for Large-Scale Energy Storage. *Adv. Mater.* **2017**, *29*, 1604007.
(3) Xue, L.; Gao, H.; Zhou, W.; Xin, S.; Park, K.; Li, Y.; Goodenough, J. B. Liquid K−Na Alloy Anode Enables Dendrite-Free Potassium Batteries. *Adv. Mater.* **2016**, *28*, 9608−9612.
(4) Wessells, C. D.; Peddada, S. V.; Huggins, R. A.; Cui, Y. Nickel Hexacyanoferrate Nanoparticle Electrodes for Aqueous Sodium and Potassium Ion Batteries. *Nano Lett.* **2011**, *11*, 5421−5425.
(5) Eftekhari, A. Potassium Secondary Cell Based on Prussian Blue Cathode. *J. Power Sources* **2004**, *126*, 221−228.

DOI: 10.1021/acsenergylett.7b01021
ACS Energy Lett. 2018, 3, 65−71

(6) Xue, L.; Li, Y.; Gao, H.; Zhou, W.; Lü, X.; Kaveevivitchai, W.; Manthiram, A.; Goodenough, J. B. Low-Cost High-Energy Potassium Cathode. *J. Am. Chem. Soc.* **2017**, *139*, 2164−2167.
(7) You, Y.; Wu, X.-L.; Yin, Y.-X.; Guo, Y.-G. High-Quality Prussian Blue Crystals as Superior Cathode Materials for Room-Temperature Sodium-Ion Batteries. *Energy Environ. Sci.* **2014**, *7*, 1643−1647.
(8) Song, J.; Wang, L.; Lu, Y.; Liu, J.; Guo, B.; Xiao, P.; Lee, J. J.; Yang, X. Q.; Henkelman, G.; Goodenough, J. B. Removal of Interstitial H_2O in Hexacyanometallates for a Superior Cathode of a Sodium-Ion Battery. *J. Am. Chem. Soc.* **2015**, *137*, 2658−2664.
(9) Wessells, C. D.; Peddada, S. V.; McDowell, M. T.; Huggins, R. A.; Cui, Y. The Effect of Insertion Species on Nanostructured Open Framework Hexacyanoferrate Battery Electrodes. *J. Electrochem. Soc.* **2012**, *159*, A98.
(10) Wessells, C. D.; Huggins, R. A.; Cui, Y. Copper Hexacyanoferrate Battery Electrodes with Long Cycle Life and High Power. *Nat. Commun.* **2011**, *2*, 550.
(11) Recham, N.; Rousse, G. l.; Sougrati, M. T.; Chotard, J.-N. l.; Frayret, C.; Mariyappan, S.; Melot, B. C.; Jumas, J.-C.; Tarascon, J.-M. Preparation and Characterization of a Stable $FeSO_4F$-Based Framework for Alkali Ion Insertion Electrodes. *Chem. Mater.* **2012**, *24*, 4363−4370.
(12) Mu, L.; Ben, L.; Hu, Y.-S.; Li, H.; Chen, L.; Huang, X. Novel 1.5 V Anode Materials, $ATiOPO_4$ (A= NH_4, K, Na), for Room-Temperature Sodium-Ion Batteries. *J. Mater. Chem. A* **2016**, *4*, 7141−7147.
(13) Fedotov, S. S.; Khasanova, N. R.; Samarin, A. S.; Drozhzhin, O. A.; Batuk, D.; Karakulina, O. M.; Hadermann, J.; Abakumov, A. M.; Antipov, E. V. $AVPO_4F$ (A= Li, K): a 4 V Cathode Material for High-Power Rechargeable Batteries. *Chem. Mater.* **2016**, *28*, 411−415.
(14) Share, K.; Cohn, A. P.; Carter, R.; Rogers, B.; Pint, C. L. Role of Nitrogen-Doped Graphene for Improved High-Capacity Potassium Ion Battery Anodes. *ACS Nano* **2016**, *10*, 9738−9744.
(15) Jian, Z.; Luo, W.; Ji, X. Carbon Electrodes for K-Ion Batteries. *J. Am. Chem. Soc.* **2015**, *137*, 11566−11569.
(16) Luo, W.; Wan, J.; Ozdemir, B.; Bao, W.; Chen, Y.; Dai, J.; Lin, H.; Xu, Y.; Gu, F.; Barone, V.; et al. Potassium Ion Batteries with Graphitic Materials. *Nano Lett.* **2015**, *15*, 7671−7677.
(17) Zhang, W.-J. A Review of the Electrochemical Performance of Alloy Anodes for Lithium-Ion Batteries. *J. Power Sources* **2011**, *196*, 13−24.
(18) Luo, W.; Jian, Z.; Xing, Z.; Wang, W.; Bommier, C.; Lerner, M. M.; Ji, X. Electrochemically Expandable Soft Carbon as Anodes for Na-Ion Batteries. *ACS Cent. Sci.* **2015**, *1*, 516−522.
(19) Jian, Z.; Xing, Z.; Bommier, C.; Li, Z.; Ji, X. Hard Carbon Microspheres: Potassium-Ion Anode Versus Sodium-Ion Anode. *Adv. Energy Mater.* **2016**, *6*, 1501874.
(20) Goodenough, J. B.; Kim, Y. Challenges for Rechargeable Li Batteries. *Chem. Mater.* **2010**, *22*, 587−603.
(21) Wang, R. Y.; Shyam, B.; Stone, K. H.; Weker, J. N.; Pasta, M.; Lee, H. W.; Toney, M. F.; Cui, Y. Reversible Multivalent (Monovalent, Divalent, Trivalent) Ion Insertion in Open Framework Materials. *Adv. Energy Mater.* **2015**, *5*, 1401869.
(22) Chen, W.; Xia, X. H. Highly Stable Nickel Hexacyanoferrate Nanotubes for Electrically Switched Ion Exchange. *Adv. Funct. Mater.* **2007**, *17*, 2943−2948.
(23) Lu, Y.; Wang, L.; Cheng, J.; Goodenough, J. B. Prussian Blue: A New Framework of Electrode Materials for Sodium Batteries. *Chem. Commun.* **2012**, *48*, 6544−6546.
(24) Tian, C.; Kan, E.; Lee, C.; Whangbo, M. H. Pi-Back-Donation Effect of the Cyanide Ligands on the Electron Correlation and Charge Transfer in Prussian Blue $RbMn[Fe(CN)_6]$. *Inorg. Chem.* **2010**, *49*, 3086−3088.
(25) Middlemiss, D. S.; Deeth, R. J. First Principles Calculation of a Large Variation in Dielectric Tensor through the Spin Crossover in the $CsFe[Cr(CN)_6]$ Prussian Blue Analogue. *J. Chem. Phys.* **2014**, *140*, 144503.
(26) Middlemiss, D. S.; Portinari, D.; Grey, C. P.; Morrison, C. A.; Wilson, C. C. Spin Crossover in the $CsFe^{II}[Cr^{III}(CN)_6]$ Prussian Blue Analog: Phonons and Thermodynamics from Hybrid Functionals. *Phys. Rev. B: Condens. Matter Mater. Phys.* **2010**, *81*, 184410.
(27) Kawamoto, T.; Asai, Y.; Abe, S. Ab Initio Calculations on the Mechanism of Charge Transfer in Co-Fe Prussian-Blue Compounds. *Phys. Rev. B: Condens. Matter Mater. Phys.* **1999**, *60*, 12990−12993.
(28) Kabir, M.; Van Vliet, K. J. Reversible Mechanism for Spin Crossover in Transition-Metal Cyanides. *Phys. Rev. B: Condens. Matter Mater. Phys.* **2012**, *85*, 054431.
(29) Wojdel, J. C.; de P. R. Moreira, I.; Bromley, S. T.; Illas, F. On the Prediction of the Crystal and Electronic Structure of Mixed-Valence Materials by Periodic Density Functional Calculations: The Case of Prussian Blue. *J. Chem. Phys.* **2008**, *128*, 044713.
(30) Wu, X.; Jian, Z.; Li, Z.; Ji, X. Prussian White Analogues as Promising Cathode for Non-Aqueous Potassium-Ion Batteries. *Electrochem. Commun.* **2017**, *77*, 54−57.
(31) Wojdel, J. C.; Bromley, S. T. Efficient Calculation of the Structural and Electronic Properties of Mixed Valence Materials: Application to Prussian Blue Analogues. *Chem. Phys. Lett.* **2004**, *397*, 154−159.
(32) Omarova, M.; Koishybay, A.; Yesibolati, N.; Mentbayeva, A.; Umirov, N.; Ismailov, K.; Adair, D.; Babaa, M.-R.; Kurmanbayeva, I.; Bakenov, Z. Nickel Hexacyanoferrate Nanoparticles as a Low Cost Cathode Material for Lithium-Ion Batteries. *Electrochim. Acta* **2015**, *184*, 58−63.
(33) Wang, Z.; Selbach, S. M.; Grande, T. Van Der Waals Density Functional Study of the Energetics of Alkali Metal Intercalation in Graphite. *RSC Adv.* **2014**, *4*, 3973.
(34) Dostal, A.; Kauschka, G.; Reddy, S. J.; Scholz, F. Lattice Contractions and Expansions Accompanying the Electrochemical Conversions of Prussian Blue and the Reversible and Irreversible Insertion of Rubidium and Thallium Ions. *J. Electroanal. Chem.* **1996**, *406*, 155−163.
(35) Okubo, M.; Honma, I. Ternary Metal Prussian Blue Analogue Nanoparticles as Cathode Materials for Li-Ion Batteries. *Dalton Trans.* **2013**, *42*, 15881−15884.
(36) Asakura, D.; Li, C. H.; Mizuno, Y.; Okubo, M.; Zhou, H.; Talham, D. R. Bimetallic Cyanide-Bridged Coordination Polymers as Lithium Ion Cathode Materials: Core@Shell Nanoparticles with Enhanced Cyclability. *J. Am. Chem. Soc.* **2013**, *135*, 2793−2799.
(37) Imanishi, N.; Morikawa, T.; Kondo, J.; Yamane, R.; Takeda, Y.; Yamamoto, O.; Sakaebe, H.; Tabuchi, M. Lithium Intercalation Behavior of Iron Cyanometallates. *J. Power Sources* **1999**, *81-82*, 530−534.
(38) Wang, L.; Lu, Y. H.; Liu, J.; Xu, M. W.; Cheng, J. G.; Zhang, D. W.; Goodenough, J. B. A Superior Low-Cost Cathode for a Na-Ion Battery. *Angew. Chem., Int. Ed.* **2013**, *52*, 1964−1967.
(39) Okubo, M.; Asakura, D.; Mizuno, Y.; Kim, J.-D.; Mizokawa, T.; Kudo, T.; Honma, I. Switching Redox-Active Sites by Valence Tautomerism in Prussian Blue Analogues $A_XMn_Y[Fe(CN)_6]\cdot nH_2O$ (A: K, Rb): Robust Frameworks for Reversible Li Storage. *J. Phys. Chem. Lett.* **2010**, *1*, 2063−2071.
(40) Wang, L.; Song, J.; Qiao, R.; Wray, L. A.; Hossain, M. A.; Chuang, Y. D.; Yang, W.; Lu, Y.; Evans, D.; Lee, J. J.; et al. Rhombohedral Prussian White as Cathode for Rechargeable Sodium-Ion Batteries. *J. Am. Chem. Soc.* **2015**, *137*, 2548−2554.
(41) Dong, H.; Li, Y.; Liang, Y.; Li, G.; Sun, C.-J.; Ren, Y.; Lu, Y.; Yao, Y. A Magnesium−Sodium Hybrid Battery with High Operating Voltage. *Chem. Commun.* **2016**, *52*, 8263−8266.
(42) Sun, X.-G.; Bi, Z.; Liu, H.; Fang, Y.; Bridges, C. A.; Paranthaman, M.; Dai, S.; Brown, G. M. A High Performance Hybrid Battery Based on Aluminum Anode and LiFePO4 Cathode. *Chem. Commun.* **2016**, *52*, 1713−1716.
(43) Walter, M.; Kravchyk, K. V.; Ibanez, M.; Kovalenko, M. V. Efficient and Inexpensive Sodium−Magnesium Hybrid Battery. *Chem. Mater.* **2015**, *27*, 7452−7458.
(44) Li, Y.; An, Q.; Cheng, Y.; Liang, Y.; Ren, Y.; Sun, C.-J.; Dong, H.; Tang, Z.; Li, G.; Yao, Y. A High-Voltage Rechargeable Magnesium-Sodium Hybrid Battery. *Nano Energy* **2017**, *34*, 188−194.

DOI: 10.1021/acsenergylett.7b01021
ACS Energy Lett. 2018, 3, 65−71

(45) Sheng, M.; Zhang, F.; Ji, B.; Tong, X.; Tang, Y. A Novel Tin-Graphite Dual-Ion Battery Based on Sodium-Ion Electrolyte with High Energy Density. *Adv. Energy Mater.* **2017**, *7*, 1601963.
(46) Zhang, X.; Tang, Y.; Zhang, F.; Lee, C. S. A Novel Aluminum–Graphite Dual-Ion Battery. *Adv. Energy Mater.* **2016**, *6*, 1502588.
(47) Ji, B.; Zhang, F.; Song, X.; Tang, Y. A Novel Potassium-Ion-Based Dual-Ion Battery. *Adv. Mater.* **2017**, *29*, 1700519.
(48) Qin, P.; Wang, M.; Li, N.; Zhu, H.; Ding, X.; Tang, Y. Bubble-Sheet-Like Interface Design with an Ultrastable Solid Electrolyte Layer for High-Performance Dual-Ion Batteries. *Adv. Mater.* **2017**, *29*, 1606805.
(49) Tong, X.; Zhang, F.; Ji, B.; Sheng, M.; Tang, Y. Carbon-Coated Porous Aluminum Foil Anode for High-Rate, Long-Term Cycling Stability, and High Energy Density Dual-Ion Batteries. *Adv. Mater.* **2016**, *28*, 9979–9985.
(50) Su, S.; NuLi, Y.; Huang, Z.; Miao, Q.; Yang, J.; Wang, J. A High-Performance Rechargeable $Mg2^{+}/Li^{+}$ Hybrid Battery Using One-Dimensional Mesoporous TiO_2 (B) Nanoflakes as the Cathode. *ACS Appl. Mater. Interfaces* **2016**, *8*, 7111–7117.
(51) Yoo, H. D.; Liang, Y.; Li, Y.; Yao, Y. High Areal Capacity Hybrid Magnesium–Lithium-Ion Battery with 99.9% Coulombic Efficiency for Large-Scale Energy Storage. *ACS Appl. Mater. Interfaces* **2015**, *7*, 7001–7007.
(52) Gao, T.; Han, F.; Zhu, Y.; Suo, L.; Luo, C.; Xu, K.; Wang, C. Hybrid $Mg2^{+}/Li^{+}$ Battery with Long Cycle Life and High Rate Capability. *Adv. Energy Mater.* **2015**, *5*, 1401507.
(53) Sun, X.; Duffort, V.; Nazar, L. F. Prussian Blue Mg-Li Hybrid Batteries. *Adv. Sci.* **2016**, *3*, 1600044.
(54) Cheng, Y.; Shao, Y.; Zhang, J.-G.; Sprenkle, V. L.; Liu, J.; Li, G. High Performance Batteries Based on Hybrid Magnesium and Lithium Chemistry. *Chem. Commun.* **2014**, *50*, 9644–9646.
(55) Cho, J.-H.; Aykol, M.; Kim, S.; Ha, J.-H.; Wolverton, C.; Chung, K. Y.; Kim, K.-B.; Cho, B.-W. Controlling the Intercalation Chemistry to Design High-Performance Dual-Salt Hybrid Rechargeable Batteries. *J. Am. Chem. Soc.* **2014**, *136*, 16116–16119.
(56) Cheng, Y.; Chang, H. J.; Dong, H.; Choi, D.; Sprenkle, V. L.; Liu, J.; Yao, Y.; Li, G. Rechargeable Mg–Li Hybrid Batteries: Status and Challenges. *J. Mater. Res.* **2016**, *31*, 3125–3141.
(57) Yao, H.-R.; You, Y.; Yin, Y.-X.; Wan, L.-J.; Guo, Y.-G. Rechargeable Dual-Metal-Ion Batteries for Advanced Energy Storage. *Phys. Chem. Chem. Phys.* **2016**, *18*, 9326–9333.

DOI: 10.1021/acsenergylett.7b01021
ACS Energy Lett. 2018, 3, 65–71